

SCC and Crevice Corrosion Inhibition of Steam Turbine ASTM A470 Steel

Behzad Bavarian, Jia Zhang and Lisa Reiner
College of Engineering and Computer Science
California State University, Northridge
Northridge, CA 91330

ABSTRACT

Localized corrosion (pitting, stress corrosion cracking and corrosion fatigue) is a leading cause of failures for low pressure steam turbines using ASTM A470 steel. Localized corrosion inhibitors can be used for protection during shutdown and routine maintenance. Commercially available corrosion inhibitors were investigated in this project to determine effectiveness of different concentrations of Inhibitor to slow down corrosion. Polarization resistance increased with concentration of corrosion inhibitor due to film formation and displacement of water molecules. Cyclic polarization behavior showed a shift in the passive film breakdown potential, indicative of more protective films. The increased strain to failure and tensile strength from the slow strain rate studies demonstrated inhibitor effectiveness at impeding SCC. The fractographic analysis showed mainly ductile overload failure. Both inhibitors increased the CPT to 45-50°C, whereas the unprotected steel showed a CPT of 8°C in 200 ppm chloride ion solutions. HE tests confirmed that the addition of these inhibitors would not cause harmful effects for the ASTM A470 steel up to $-2.0 V_{SCE}$. The corrosion inhibition mechanism was determined to best fit the Langmuir adsorption isotherm with enthalpy of adsorption ranging from -14 to -18 kJ/mol. This suggests the inhibitor physically adsorbs to the metal surface which would provide suitable protection, given that the majority of corrosion damage to turbo-machinery systems occurs during the shutdown period due to chemistry changes and stagnant conditions in localized areas.

Keyword: SCC, Critical pitting temperature, Steam turbine, Volatile Corrosion Inhibitors, physisorption

INTRODUCTION

Steam turbine rotors are critical components in power plants. Low pressure rotors are typically constructed from forged ASTM A470¹, 3.5NiCrMoV (class 2 to 7), while shrunk-on disks are made of ASTM A471² (class 1 to 3). The strength and hardness of turbine rotors, discs and blades is limited because the stronger and harder materials are highly susceptible to stress corrosion cracking (SCC), hydrogen embrittlement (HE), and corrosion fatigue (CF). The initial events in localized corrosion damage, such as pitting on blade and disk alloy surfaces often lead to sudden and catastrophic failures in low pressure (LP) steam turbines. The consequences of a rotor failure impact safety and economics. Turbine cracking generally occurs where the flowing steam (gas phase) begins to transform to the liquid phase³⁻⁶ and cracking can occur where the flow of steam is stagnant. This outcome indicates that condensation of corrosive chemicals changes the environment and induces crack initiation. The crack propagation rate increases with yield strength due to increased susceptibility to hydrogen embrittlement. This susceptibility limits the use of high strength materials for turbine discs in power plants (yield strength below 965 MPa (140 ksi) is recommended). For ASTM A470 corrosion protection is extremely critical to maintain functionality of these systems. As a result, the development of effective localized corrosion inhibitors is essential for downtime environments in steam turbines or other complex industrial systems. The majority of damages occur during the shutdown period due to the chemistry changes and stagnant conditions in localized areas. The likelihood of corrosion onset is influenced by the presence of corrosive species, temperature and pH during the shutdown. Increased chloride ion concentration and changes in pH affect the stability of the protective oxides and eventually its breakdown, resulting in pit nucleation. Accumulation of localized corrosion damage is preceded by passivity breakdown and pit nucleation, given the stated corrosive environment in LP steam turbines within the phase transition region.^{3, 7-9}

The nucleation and development of deposits on blade surfaces can reduce turbine efficiency and promote the formation of corrosive environments. In general, it is believed that by lowering chloride ion concentration below 35 ppm, the susceptibility to localized corrosion decreases significantly. If chloride concentration on the surface is reduced immediately upon shutdown, this will provide a corrective strategy for minimizing or even eliminating the failure of discs and blades. This is most easily accomplished by washing the blade and disc surfaces with chloride-free water. In fact, an even more effective strategy would be to combine turbine surface washing with dehumidification or nitrogen blanketing. For the accessible surfaces, this strategy can work, but for crevices, notches and cavities, it is difficult to reach these surfaces. Accumulation of corrosive species and pH changes inside these restricted geometries can alter the electrochemical reactions to initiate pitting or crevice corrosion that eventually leads to SCC and corrosion fatigue. The effects of inhibitor concentration and temperature on the stress corrosion cracking of turbine steels were investigated in this project.

Turbo-machinery maintenance

Turbo-machinery systems have regular service maintenance and unexpected shut downs. During scheduled service maintenance, components are frequently washed to dilute or remove any in service contaminants (salt, dirt, grease and oil). There are three main types of cleaning: aqueous, organic solvent and abrasive. Aqueous cleaning covers a wide variety of cleaning methods (detergents, acids and alkaline compounds) to displace soil. Improved corrosion prevention compounds and coating systems can protect the sensitive alloy from the environment. These coatings, combined with improved repair and maintenance procedures, will ensure adequate performance of equipment manufactured from an SCC sensitive alloy. The most costly, yet best method for eliminating SCC is to replace the material with an alloy specifically designed to resist this form of corrosion. The inhibitors investigated in this program are biodegradable compounds that blend amine salts, carboxylic acid and a wetting agent (surfactant) in a water solution. Wetting agents are added to maintain aminocarboxylates on the metal surface. The compounds alter hydrocarbons (grease) so that the deposits can be removed with water. Any conventional cleaning equipment (power washers, steam cleaners, dip tanks) can be used for multi-metal corrosion protection.

Vapor phase corrosion inhibitors

Several groups of organic compounds have shown corrosion inhibition properties. Most of the effective organic compounds contain oxygen, sulfur, phosphorus or nitrogen atoms, and in terms of structure, have triple bonds and aromatic rings to improve the inhibitor's adsorption to the metal surface.^{10, 11} Organic inhibitors can protect by adsorbing to the metal surfaces, molecules attach directly to the surface, in a very thin layer (monomolecular), and do not penetrate into the bulk of the metal. The extent of adsorption of an inhibitor depends on many factors: 1) the nature and the surface charge of the metal; 2) the Inhibitor-Adsorption mode; and 3) the inhibitor's chemical structure. Volatile Corrosion Inhibitors (VCI) deposit protective vapors on surfaces, in cracks, pits and crevices, then condense to form a thin barrier film. VCI can also neutralize the pH and other corrosive species, which is an effective way to reduce acidity of the local chemistry inside a turbine system.

VCIs, frequently, are a complex mixture of amine salts and aromatic sulfonic acids that provide direct contact inhibition and incorporate volatile carboxylic acid salts as a vapor phase inhibitor for metal surfaces not sufficiently coated. The thin polar layer of surfactants is tightly bound to the metal surface through chemisorption or physisorption. Between this thin polar layer and the corrosive environment is the thicker barrier layer of hydrocarbons. The sulfonate part of the inhibitor displaces water from the metal surface and promotes adsorption of inhibitor to the surface. Active sites with complimentary energy levels to the polar group energy levels form a tighter, more uniform layer over the metal surface. The barrier layer has three important characteristics: 1) low permeability by moisture; 2) compatibility with the oleophilic ends of the polar layer molecules so that the barrier is held firmly in place; and 3) good solubility in the carrier to attach the polar and barrier layers to the metal surface. The VCI film barrier replenishes through further evaporation and condensation of the inhibitor on the metal surface. VpCI-337⁽¹⁾ (Inhibitor-A) is a ready-to-use waterborne corrosion inhibitor for indoor use. The vapor phase corrosion inhibitors in Inhibitor-A migrate and protect metal surfaces, resulting in time and cost savings. Inhibitor-A is effective on ferrous metals as well as aluminum and plated steels. EcoLine 3690⁽²⁾ (Inhibitor-B) is a biodegradable, bio-based, ready-to-use temporary coating, designed for severe marine and high humidity conditions. When applied to the surface, this product leaves an oily film, which provides excellent protection for any metal surface. The film is self-healing and moisture displacing, providing superior protection against aggressive environments. It is a mixture of sulfonates, hydrocarbon waxes and amine salt of fatty acid in an oil carrier.

An adsorption isotherm is a mathematical function that relates the surface coverage of a chemical on a surface (usually a metal) to the concentration of the chemical. Identification of the surface adsorption isotherm is important and can lead to the determination of a mechanism. It is assumed that the corrosion current density, which is directly related to the corrosion rate, is representative of the number of corrosion sites. Therefore, adding inhibitor to the environment should diminish the number of corrosion initiation sites by displacing water molecules on the surface with inhibitor molecules, thereby decreasing the corrosion rate. In recent years, electrochemical and weight loss methods that relate the corrosion current density or the amount of weight loss with the inhibitor coverage have been used to study adsorption and the corrosion inhibition of various materials on a metallic surface.^{13, 14} Many models for adsorption isotherms have been defined (Temkin, Freundlich, Langmuir and Frumkin). Each of these adsorption isotherms explains a different type of relationship between concentration and surface coverage of an inhibitor on a metal or alloy surface.^{10, 11, 14} Based on the adsorption isotherm graph, the adsorption equilibrium constant, K_{ad} , can be calculated. Identifying the adsorption equilibrium constant, can lead to the calculation of the free standard energy of adsorption, $\Delta G_{ad} = -RT \ln (K_{ad})$. By repeating the same experiment at different temperatures, the enthalpy of the adsorption, ΔH_{ad} can be calculated.

⁽¹⁾Trade name, ⁽²⁾Trade name

EXPERIMENTAL PROCEDURE

Corrosion inhibition of Inhibitor-A and Inhibitor-B (two commercially available inhibitors) was investigated for ASTM A470 steel in turbo-expander and steam/gas turbine applications. ASTM A470 is common steel for low pressure steam turbine disc/rotor. Its chemical composition consists of 3.5% Ni, 1.5% Cr, 0.8 % Mo, 0.25% V. The test samples were annealed at 850°C for 24 hours and air cooled, to achieve a hardness of 32 R_C. After heat treatment the mechanical properties obtained were: tensile strength of 965 MPa (140 ksi), yield strength of 826 MPa (120ksi) and Elongation of 15%. Electrochemical polarization standards per ASTM-G61¹⁵ and G150 critical pitting temperature were used to evaluate the electrochemical behavior of these inhibitors on ASTM A470 steel. These techniques can provide useful information regarding the corrosion mechanisms, corrosion rate and localized corrosion susceptibility of a material in a given environment. The studies were conducted using Gamry PC4/750™ instrumentation and DC105 corrosion test software. Samples were polished (600 grit) placed in a flat cell and tested in different inhibitor concentrations with deionized water and 200 ppm Cl⁻ solutions. A series of cyclic polarization tests were performed in temperatures ranging from 20 °C to 60 °C. Electrochemical impedance spectroscopy (EIS300™) software was used to investigate the inhibitor effectiveness of the steel alloy and gather data for adsorption isotherms in different inhibitor concentrations of deionized water containing 200 ppm Cl⁻. The R_p, polarization resistance value (determined from the Bode plot) was used to fit the data into adsorption isotherm models.

Crevice Corrosion Investigation

ASTM A470 was tested in an eight-station alternate immersion system. The samples were immersed in various concentrations of corrosion inhibitor, sodium chloride (Cl⁻) and tap water. Alternate immersion, an aggressive procedure, was performed to evaluate the inhibitor's ability to build resistance to crevice corrosion. The testing cycle immersed the samples for 10 minutes, then exposed them to air for 50 minutes per ASTM G44 and G48.^{16, 17} After 200 cycles of testing, the samples were disassembled, examined and photographed to document crevice corrosion resistance.

SCC Investigation

The slow strain rate tests were conducted on cylindrical samples under controlled electrochemical conditions using a strain rate of $5 \times 10^{-7} \text{ cm sec}^{-1}$. To evaluate the inhibitor's effectiveness, these alloys were tested in a 1.0% to 10.0% VCl solution (a typical concentration recommended to reduce localized corrosion attack) and the control samples were tested in tap water and +200 ppm Cl⁻ solutions without inhibitor. To determine the degree of inhibitor effectiveness, cathodic and anodic potentials of -2000 to +1000 mV_{SCE} sec⁻¹ were applied to the samples during the test to study how these inhibitors will function.

RESULTS

Cyclic Polarization Behavior

Figure 1 and Table 1 show the polarization behavior for ASTM A470 steel in varying concentrations (1, 5 and 10%) of Inhibitor-A with 200 ppm Cl⁻. The most noticeable changes are the positive shift in the breakdown potentials and expansion of the passive range for this steel in Inhibitor-A. The inhibitor changed the reactivity by reducing the pH level, increased the passivation range significantly, and had beneficial consequences for reducing localized corrosion damages. Table 2 shows the cyclic polarization behavior for a modified ASTM G-61 procedure with the steel samples in previously stated solution concentrations at steam turbine temperatures ranging between 30 to 50°C. As demonstrated in these polarization curves, extension of the passive zone contributes to the stability of the protective oxide film over a wider electrochemical range, resulting in a more stable passive film.

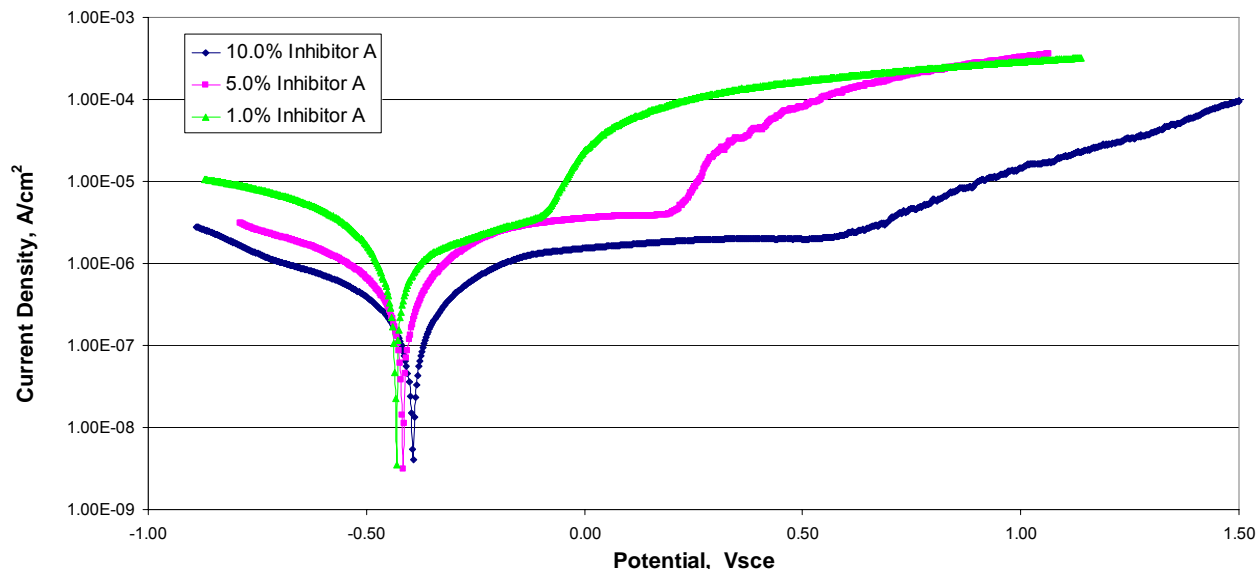


Figure 1: Electrochemical polarization behavior of ASTM A470 Steel in different Inhibitor-A concentration with 200 ppm chloride ions.

Table 1: Electrochemical behavior of ASTM A470 Steel in 200 ppm Cl^- and varying concentrations of Inhibitor-A.

Sample	E_c , mV _{SCE}	I_c uA/cm ²	E_b , mV _{SCE}	CR, mpy	Passive range mV _{SCE}	I_{pss} uA/cm ²
200 ppm Cl^- +						
+0.0 % Inhibitor-A	-675	1.470	-450	0.63	none	NA
+1.0% Inhibitor-A	-460	0.389	+45	0.17	-300 to +20	3.12
+5.0% Inhibitor-A	-415	0.304	240	0.13	-200 to +200	3.22
+10.0% Inhibitor-A	-392	0.083	1060	0.04	-100 to +950	1.92

Table 2: Effects of temperature on electrochemical behavior of ASTM A470 Steel in 200 ppm Cl^- and 1.0% or 5.0% concentration Inhibitor-A.

Solutions	Temp °C	E_c mV _{SCE}	I_c uA/cm ²	E_b mV _{SCE}	CR mpy	Passive range mV _{SCE}	I_{pss} uA/cm ²
200 ppm Cl^- +							
0.0% Inhibitor-A	30	-675	1.47	-450	0.63	none	NA
1.0% Inhibitor-A	30	-460	0.389	+45	0.17	-300 to +20	3.12
1.0% Inhibitor-A	40	-415	0.492	+70	0.21	-300 to +75	3.82
1.0% Inhibitor-A	50	-430	0.463	+130	0.20	-300 to +120	2.47
5.0% Inhibitor-A	30	-415	0.304	+240	0.12	-200 to +200	3.57
5.0% Inhibitor-A	40	-450	0.31	+320	0.13	-200 to +300	4.20
5.0% Inhibitor-A	50	-460	0.221	+430	0.09	-200 to +420	3.02

Electrochemical impedance spectroscopy, EIS (ASTM G106)¹⁸ test results are summarized in Table 3 and Figure 2. Inhibitor-A increased the resistance polarization. The increased polarization resistance can be attributed to the film formation on the metal surfaces and its ability to neutralize the corrosive species. Similar inhibition effectiveness was observed for Inhibitor-B (Table 4 and Figure 3).

Figures 4-5 show critical pitting temperature (CPT) information for the steel samples at varying anodic potentials and Inhibitor-A concentrations. Figure 6 shows similar information for Inhibitor-B. Both inhibitors increased the CPT to 45-50°C, whereas the unprotected steel showed a CPT of 8°C in 200 ppm chloride ion solutions.

Table 3: Rp values for ASTM A470 Steel determined from EIS in different concentrations of Inhibitor-A.

	Inhibitor-A Concentration (%)		
	0.0%	1.0%	5.0%
ASTM A470	Rp value (Kohms)		
in water	5.01	1,600	2,430
in 200 ppm Cl ⁻	2.80	220	766

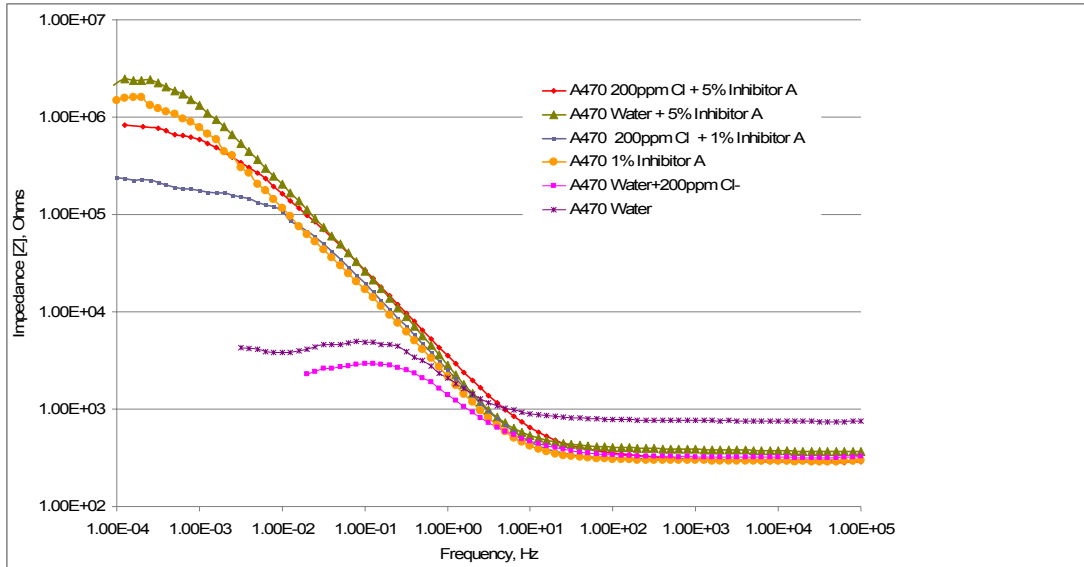


Figure 2: Electrochemical impedance spectroscopy Bode plots for ASTM A470 Steel in different Inhibitor-A concentrations.

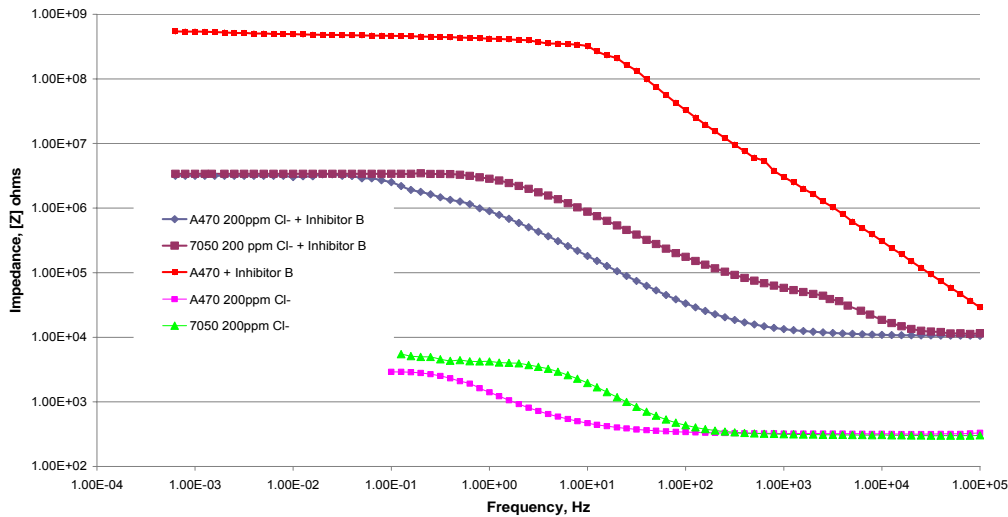


Figure 3: Electrochemical impedance spectroscopy Bode plots for ASTM A470 steel coated with Inhibitor-B and tested in 200 ppm Cl⁻ solutions.

Table 4: Rp values for ASTM A470 generated by EIS in +200ppm Cl⁻ coated with Inhibitor-B.

Alloy	Inhibitor-B	
	Non-coated (kohms)	Coated (kohms)
ASTM A470	2.8	34,000

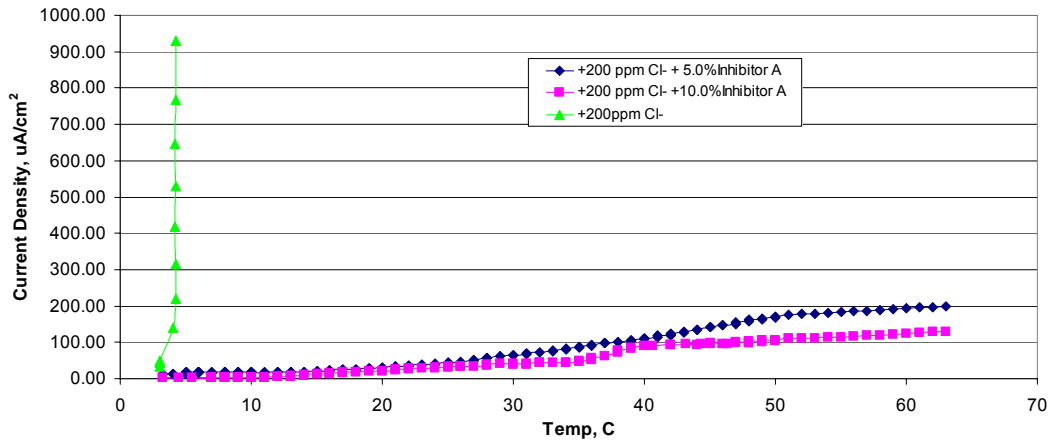


Figure 4: Critical Pitting Temperature determination for ASTM A470 steel in several Inhibitor-A concentrations at applied potential of +0.2 V_{SCE} per ASTM G150.

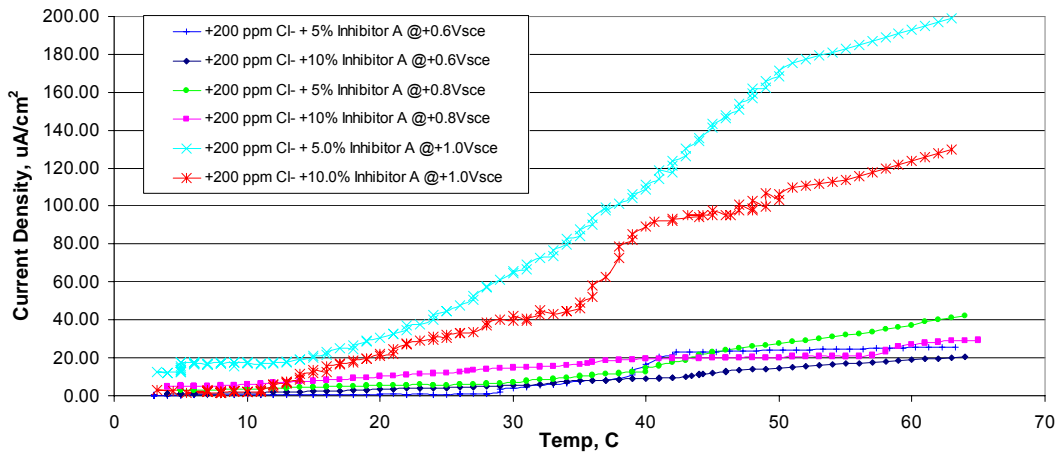


Figure 5: Critical Pitting Temperature tests for ASTM A470 steel in several Inhibitor-A concentrations at varying applied anodic potentials per ASTM G150.

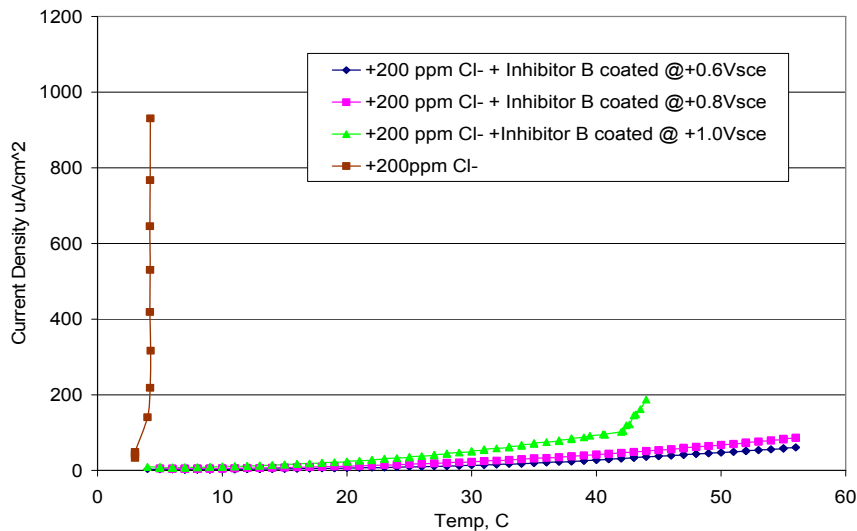


Figure 6: Critical Pitting Temperature tests for ASTM A470 steel in several Inhibitor-B concentrations at different applied anodic potentials per ASTM G150.

Crevice Corrosion

Figure 7 show photos of ASTM A470 samples after 200 hours of alternate immersion in various solutions. The samples immersed in tap water and +200 ppm Cl⁻ show severe corrosion damage. The corrosion damage lessened with the addition of inhibitor to the testing environments. The passive film stability has improved the corrosion resistance for the inhibitor treated samples. Coated samples with Inhibitor-B showed no sign of corrosion attack. Due to the hydrophobic nature of this inhibitor, aggressive species could not wet the surface, resulting in excellent corrosion protection.

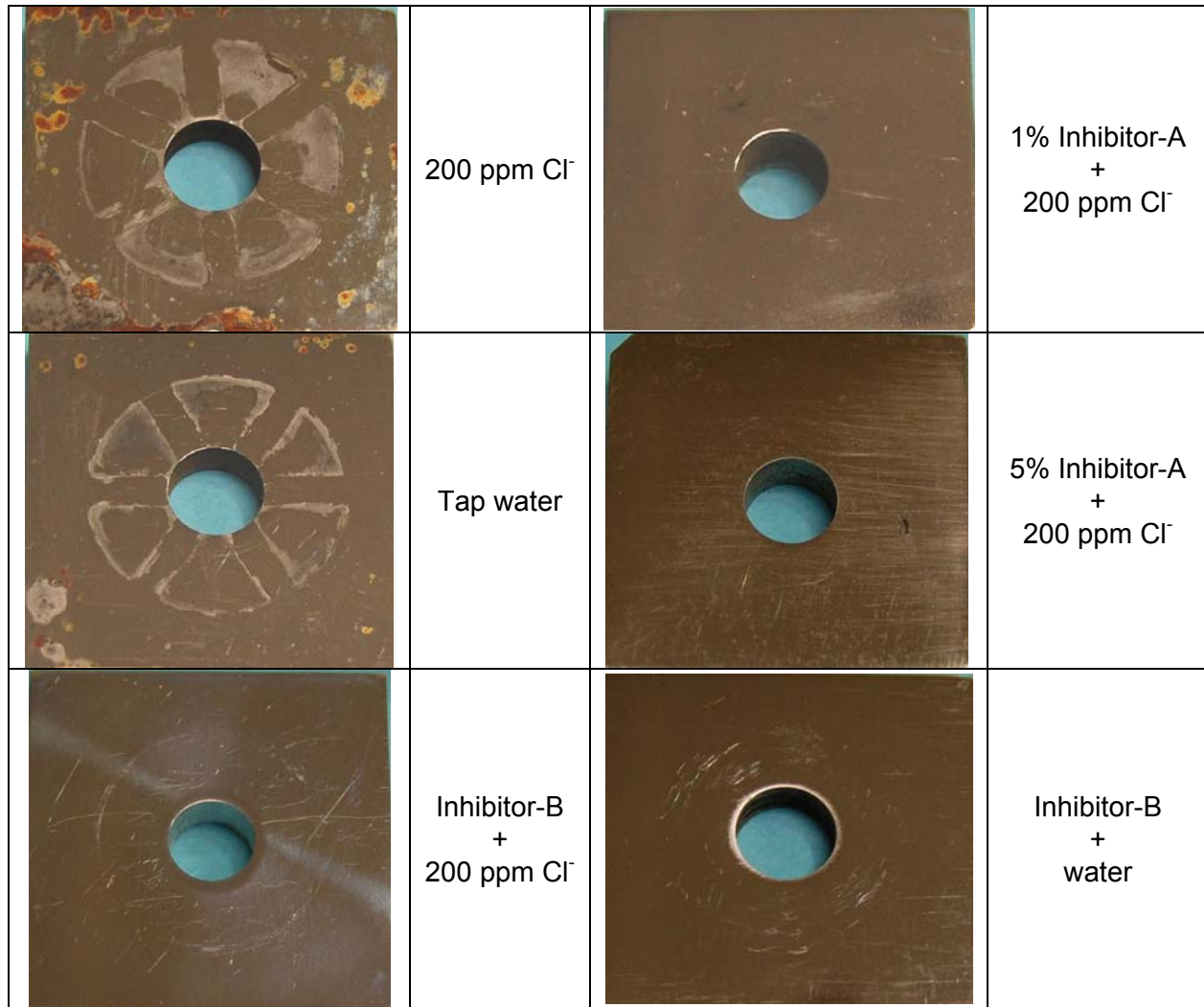


Figure 7: Crevice corrosion tests on ASTM A470 in alternate immersion for 200 hours.

Stress Corrosion Cracking

Susceptibility to SCC was determined for this steel alloy using the slow strain rate test per ASTM G129 (at a rate of 5×10^{-7} cm per second).¹⁹ At applied potentials close to the passive film breakdown potential, a noticeable increase in susceptibility was seen for the samples tested without inhibitor. The greatest reduction in degree of susceptibility is seen around -200 mV_{SCE} for steel. Figures 8-9 show the SCC test results for ASTM A470 steel. Greater ductility is seen for the samples tested in 5.0% concentration Inhibitor-A (5.0% Inhibitor A) and the sample tested in air (no corrosive medium). Figure 9 show the results for samples tested in Inhibitor-B at cathodic and anodic potentials with comparable strength and ductility to samples tested with no solution (air). The worst performance was seen for the sample tested without inhibitor in a solution of water and 200 ppm chloride ions, where the strain was roughly 8%. Figures 10-11 show a bar graph where values for susceptibility less than 0.75 are considered to have

higher degree of susceptibility to corrosion (undesirable). In the presence of 5.0% Inhibitor-A, fractographs showed mainly ductile overload failure with significantly less localized corrosion damage except at aggressive anodic potentials higher than $-200 \text{ mV}_{\text{SCE}}$ (Figures 12-15). 5.0% Inhibitor-A solutions behaved similar to an inert environment. ASTM A470 steel showed morphology with intergranular attack for the samples tested in uninhibited solutions (Figure 13). Samples tested with a coating of Inhibitor-B showed mainly ductile overload failure with no localized corrosion damage at applied potential of $-200 \text{ mV}_{\text{SCE}}$. The slow strain rate tests showed that Inhibitor-A and -B provide effective protection in the anodic potential range.

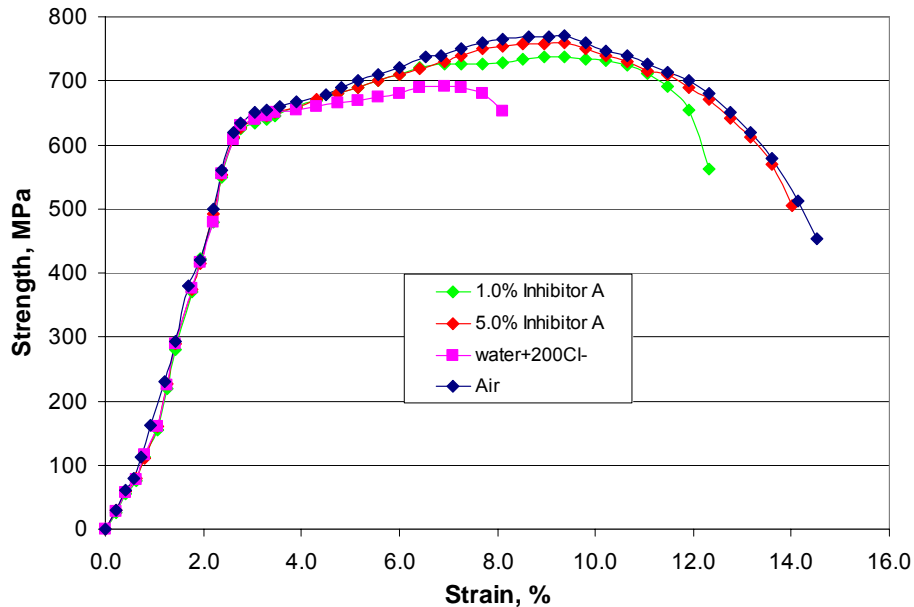


Figure 8: The slow strain rate test results for steel per ASTM G129 after SCC tests in different solutions of water, Inhibitor-A and 200 ppm Cl^- at $200 \text{ mV}_{\text{SCE}}$.

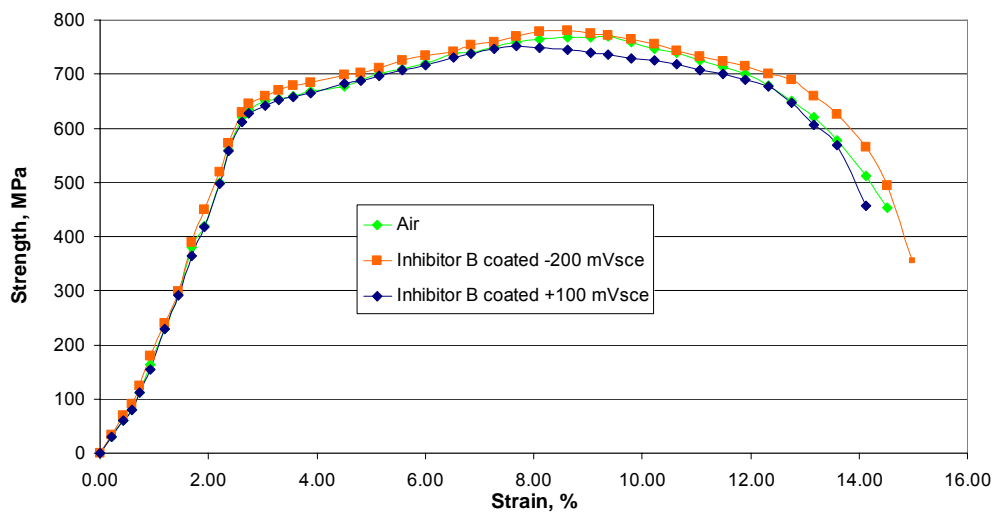


Figure 9: The slow strain rate test ($5 \times 10^{-7} \text{ cm/sec}$) results for Inhibitor-B coated steel samples in water and 200 ppm Cl^- showed very effective SCC inhibition.

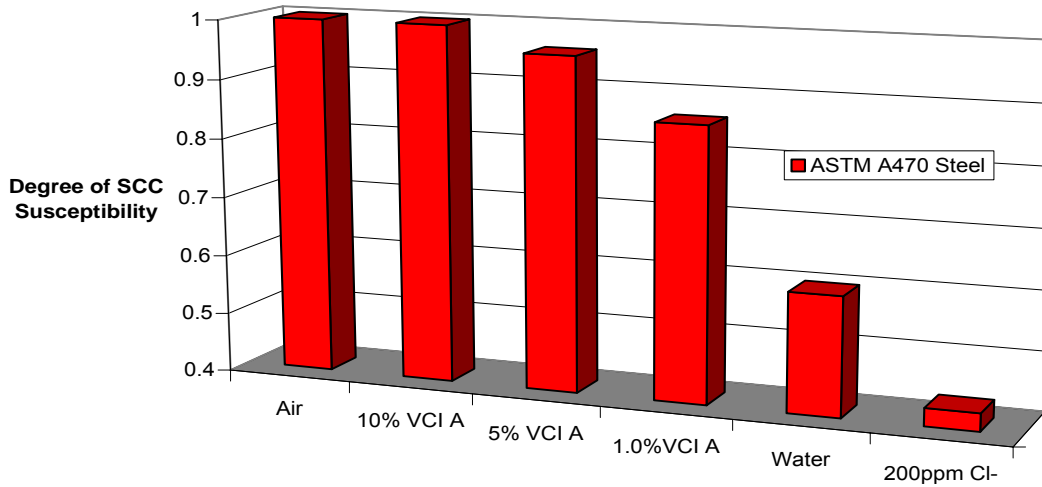


Figure 10: Comparison of SCC susceptibility of ASTM A470 in different solutions obtained from slow strain rate testing at an applied potential of $-200\text{ mV}_{\text{SCE}}$.

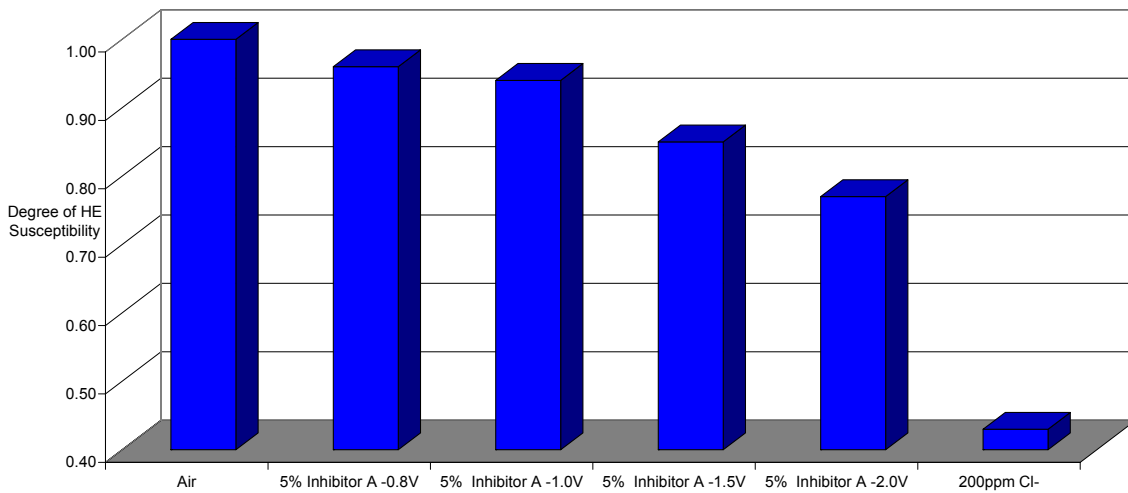


Figure 11: Slow strain rate tests ($5 \times 10^{-7}\text{ cm/sec}$) for ASTM A470 steel in several Inhibitor-A concentrations at varying cathodic potentials per ASTM G129.

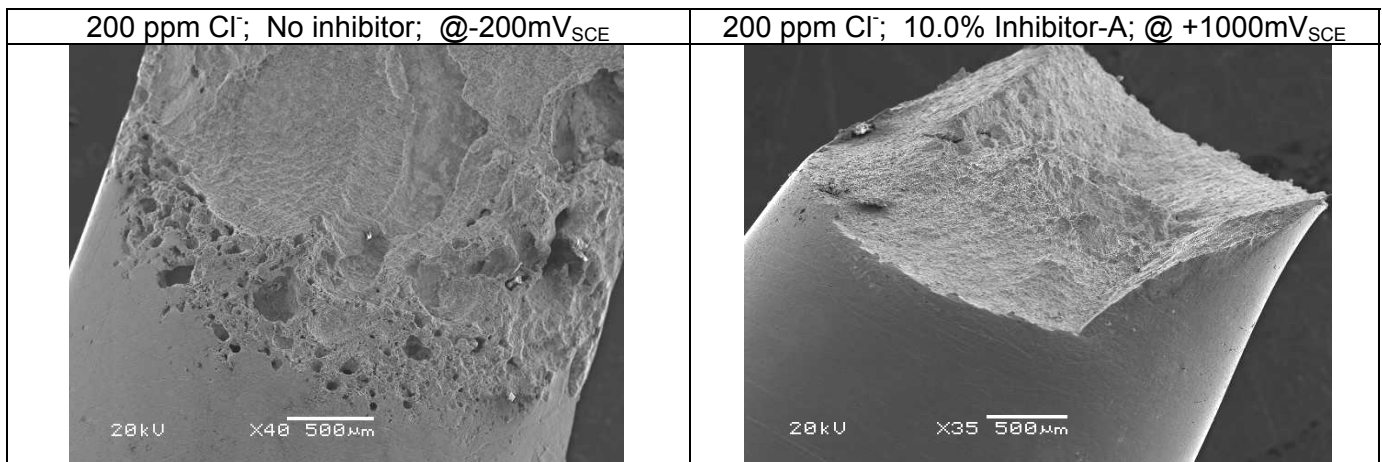


Figure 12: SEM micrographs of the fracture surface for ASTM A470 steel after SCC tests in different electrochemical conditions, showing significant corrosion resistance in presence of Inhibitor-A.

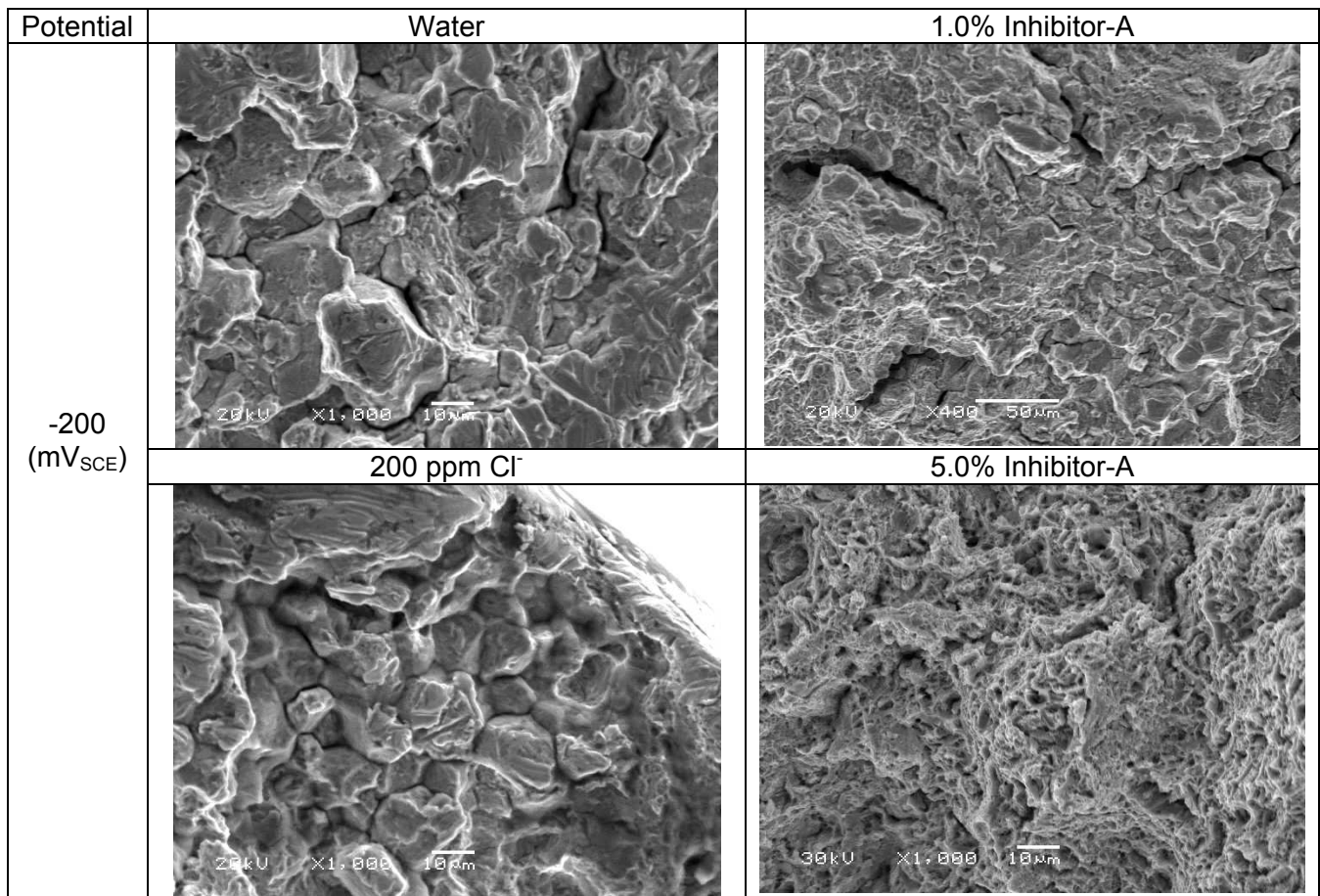


Figure 13: SEM micrographs of the fracture surface for ASTM A470 steel after SCC tests in different electrochemical conditions

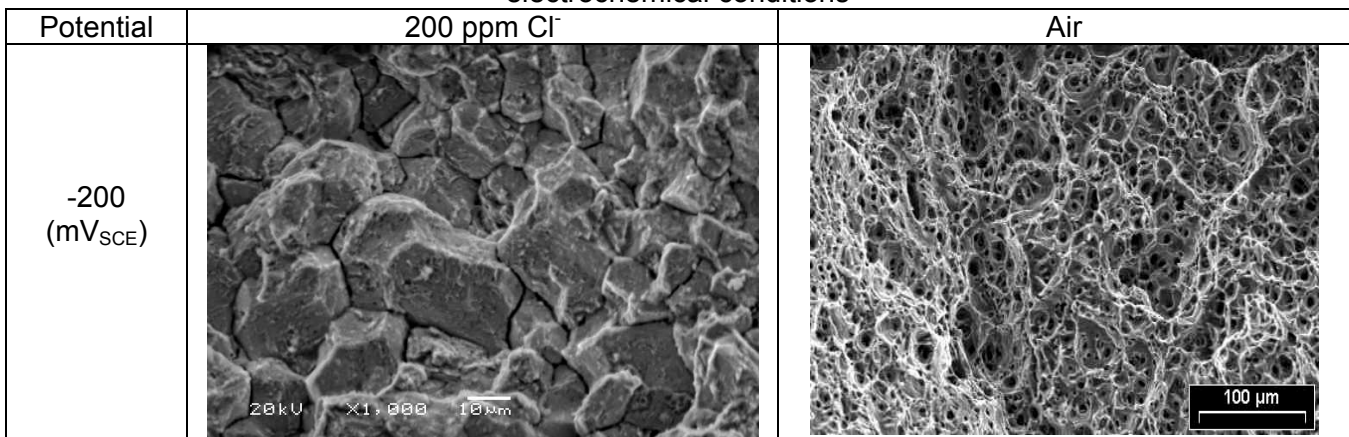


Figure 14: SEM micrographs of the fracture surface for ASTM A470 after SCC tests in different electrochemical conditions.

Figure 11 shows graph comparing hydrogen embrittlement (HE) susceptibility for Inhibitor-A. These tests confirmed that the addition of these inhibitors would not cause harmful effects for the ASTM A470 steel up to $-2.0 V_{SCE}$. The inclusion of 10% Inhibitor-A reduced susceptibility to SCC and HE for steel in a wide potential range of -2.0 to $+1.0 V_{SCE}$. The fractographs seen in Figures 15-17 demonstrate the ductile overload failure morphology for the steel samples tested in corrosive environments (chloride ions and sulfur) with inhibitor as compared to the intergranular failure surfaces seen for samples with no inhibitor.

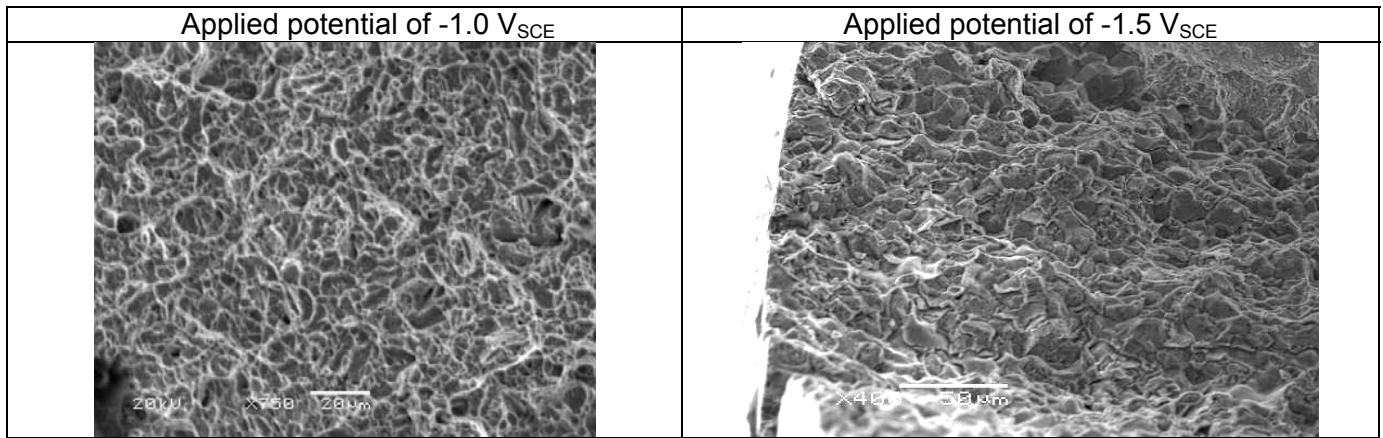


Figure 15: SEM micrographs of the fracture surface for ASTM A470 steel after SCC tests in solution of 200 ppm chloride ions, 50 ppm sulfur +10% Inhibitor-A; shows significant corrosion resistance in presence of Inhibitor-A.

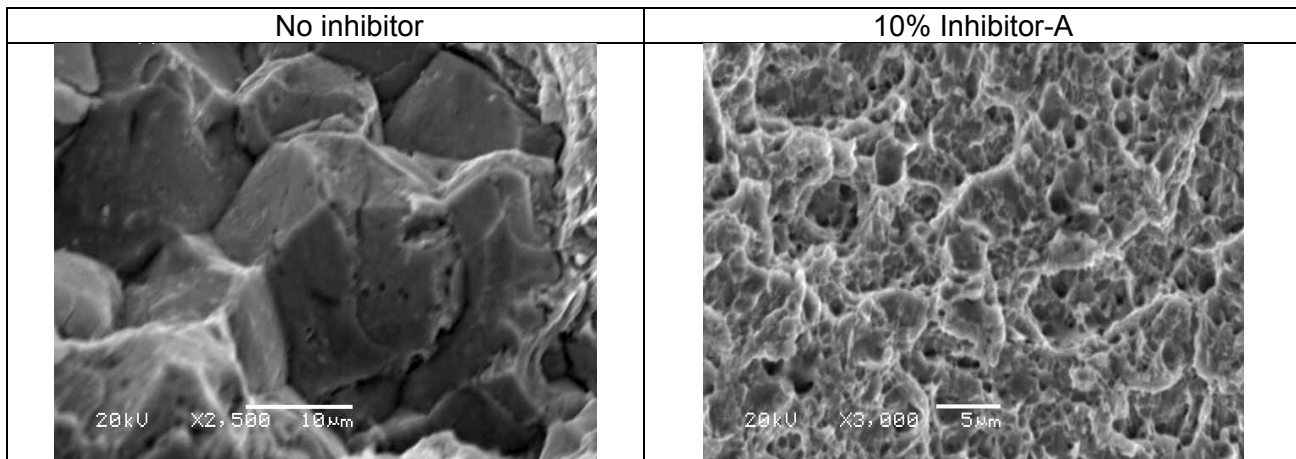


Figure 16: SEM micrographs of the fracture surface for ASTM A470 steel after SCC tests in solution of 200 ppm chloride ions, 50 ppm sulfur (pH 2.6) at applied potential of $-1.0 V_{SCE}$.

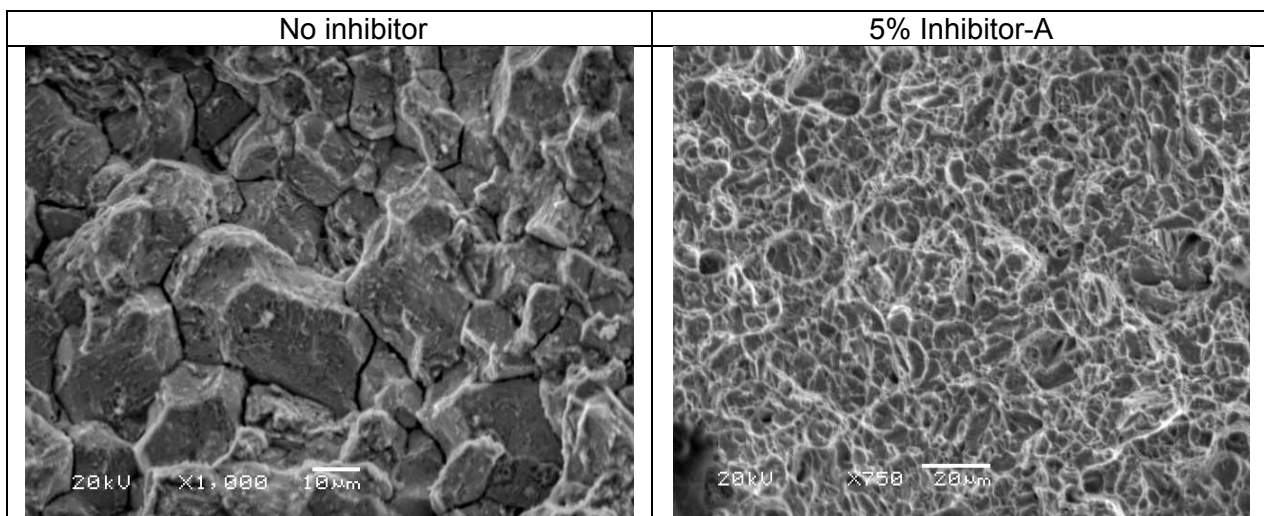


Figure 17: SEM micrographs of the fracture surface for ASTM A470 steel after SCC tests in solution of 200 ppm chloride ions at applied potential of $-0.2 V_{SCE}$.

Verification of the Inhibition Mechanism

The corrosion inhibition mechanism of Inhibitor-A was investigated using the data acquired from the EIS tests. EIS, when modeled correctly, is a powerful tool for analysis of complex electrochemical systems. A modified Randles model was used to obtain the polarization resistance (R_p) values. The Bode plots show that Inhibitor-A increases the polarization resistance of the steel alloys (Figure 2 and Table 3) with higher inhibitor concentrations resulting in higher R_p values. The increased polarization resistance can be attributed to the adsorption of inhibitor molecules to the metal surfaces. The addition of inhibitor has increased the R_p value from 2.8 k Ω for ASTM A470 in the blank solution (0 ppm concentration) to 220 k Ω for 1.0% Inhibitor-A, and 766 k Ω for 5.0% Inhibitor-A (Table 3). The high R_p value is due to the progressive adsorption of inhibitor molecules and film formation on the metal surface. The data obtained from the EIS experiment best fit the Langmuir adsorption isotherm, where $\ln(\text{concentration})$ vs. $[\ln\theta - \ln(1-\theta)]$ resulted in good linearity. The important thermodynamic values (changes in enthalpy of adsorption and changes in free standard energy of adsorption) can be obtained with adsorption isotherms and classical thermodynamics. The value of ΔG_{ad} could be used to identify the adsorption mechanism. In chemical adsorption, ΔG_{ad} is usually much higher than physical adsorption. The criterion for chemical adsorption varies depending on the paper referenced;¹¹ the range is stated to be between -40 kJ/mol and -100 kJ/mol energy. Physical adsorption requires energy between -5 to -20 kJ/mol.⁷

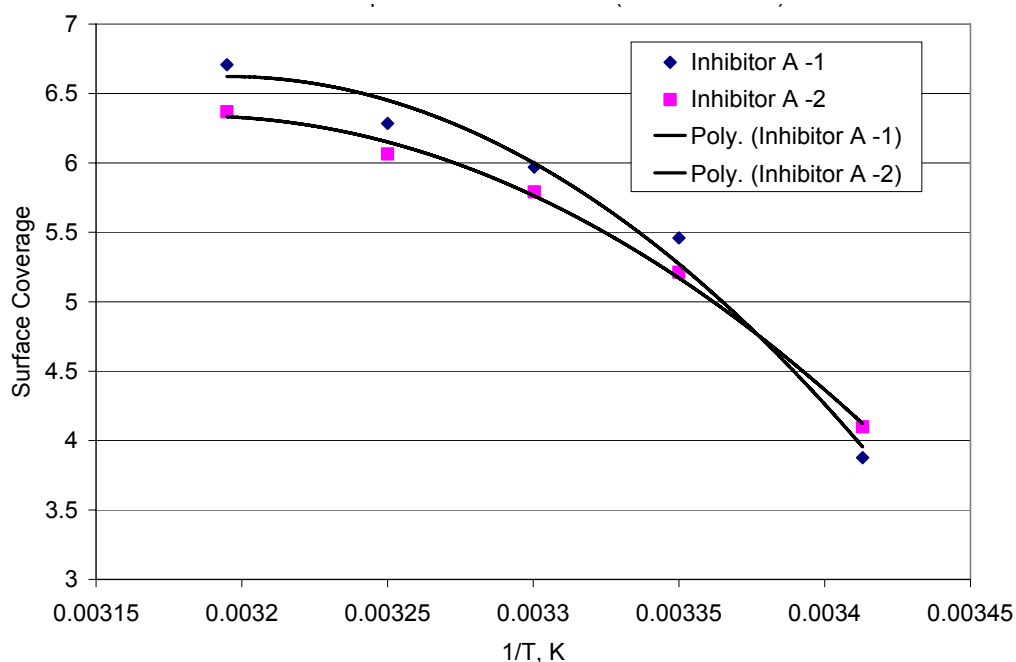


Figure 18: Langmuir adsorption isotherm showing the relationship between surface coverage and Inhibitor-A concentration on the surface of the ASTM A470 steel (two sets of data).

The analysis of Inhibitor-A showed the enthalpy of adsorption to be roughly -14 to -18 kJ/mol (Figure 18); this would indicate that the inhibitor has strong physical adsorption to the metal surface. Generally, chemisorption makes strong bonding between the Inhibitor-A and the surface of the substrate, resulting in a more stable protective film. The majority of corrosion damage to turbo-machinery systems, however, occurs during the shutdown period due to chemistry changes and stagnant condition in localized areas. Therefore, a corrosion inhibitor with strong physical adsorption to the metal surface will provide satisfactory protection.

CONCLUSIONS

A comprehensive investigation was undertaken to characterize the corrosion behavior of turbo-machinery systems in vapor phase corrosion inhibitors. Effectiveness of two commercially available inhibitors was confirmed with electrochemical impedance spectroscopy, cyclic polarization, and critical pitting temperature in room temperature and elevated temperature studies. As well, identification of the adsorption mechanism and corrosion activation energy was explored. The data acquired from EIS tests showed that Inhibitor-Adsorption to these alloy surfaces fits with the Langmuir adsorption isotherm; the enthalpy of adsorption is approximately -14 to -18 kJ/mol which suggests a strong physisorption compound. Cyclic polarization behavior for samples in the vapor phase inhibitors showed a significant upward shift in the passive film breakdown potential. This increase in the passive film range will improve localized corrosion resistance. Both inhibitors increased the CPT to 45-50°C, whereas the unprotected steel showed a CPT of 8°C in 200 ppm chloride ion solutions.

Crevice corrosion test results showed improved corrosion inhibition behavior compared with unprotected samples. The SCC susceptibility degree from the stress corrosion cracking studies showed significant reduction in SCC susceptibility in environments with added Inhibitor-A. Furthermore, ductile overload failure mode was observed for the alloys tested in the 5% Inhibitor-A and Inhibitor-B coating. HE tests confirmed that the addition of these inhibitors would not cause harmful effects for the ASTM A470 steel up to $-2.0 V_{SCE}$.

In summary, both inhibitors provide effective corrosion protection for ASTM A470 steel blades and discs used in low pressure steam turbines during the shutdown period.

ACKNOWLEDGEMENTS

The authors would like to express their appreciation to the W.M. Keck Foundation, AHPCRC and Cortec Corp. for their sponsorship of this project.

REFERENCES

1. ASTM A470, "Standard Specification for Vacuum-Treated Carbon and Alloy Steel Forgings for Turbine Rotors and Shafts" (West Conshohocken, PA: ASTM).
2. ASTM A471, "Standard Specification for Vacuum-Treated Alloy Steel Forgings for Turbine Rotor Disks and Wheels" (West Conshohocken, PA: ASTM).
3. O. Jonas and L. Machemer, Steam Turbine Corrosion and Deposits Problems and Solutions, Proceedings of the 37th Turbomachinery Symposium, 2008.
4. T. H. McCloskey, R. B. Dooley, and W. P. McNaughton, Turbine Steam Path Damage: Theory and Practice, Vols 1 and 2, Electric Power Research Institute, Palo Alto, CA, 1999.
5. Y. Zhang D. Macdonald and M. Urquidi-Macdonald, George R. Engelhardt and R. Barry Dooley, Passivity breakdown on AISI Type 403 stainless steel in chloride-containing borate buffer solution, Corrosion, 48, 354 (1992).
6. G. Engelhardt and D. Macdonald, Deterministic Prediction of Corrosion Damage in Low Pressure Steam Turbines, Corrosion Science, 46, 2755: 2004.
7. O. Jonas, J.M. Mancini, Materials Performance 40 (3) (2001) 48–53.
8. A. Turnbull and S. Zhou, Comparative evaluation of environment induced cracking of conventional and advanced steam turbine blade steels. Part 1: Stress corrosion cracking, Corrosion Science 52 (2010) 2936–2944.
9. A. Turnbull and S. Zhou, Pit to crack transition in stress corrosion cracking of a steam turbine disc steel, Corrosion Science, Vol 46, 1239 (2004).

10. F. Bentiss, B. Mernari, M. Traisnel, H. Vezin and M. Lagrenée, On the relationship between corrosion inhibiting effect and molecular structure of 2,5-bis(n-pyridyl)-1,3,4-thiadiazole derivatives in acidic media: AC Impedance and DFT studies, Corrosion Science 53 (2011) 487–495.
11. R. Gasparac, C. R. Martin and E. Stupnisek-Lisac, In situ Studies of Imidazole and its Derivatives as Copper Corrosion Inhibitors, Journal of The Electrochemical Society, 147 (2) 548-551 (2000).
12. D. Jones, Principles and Prevention of Corrosion (2nd Edition), Prentice Hall, Inc, 1996.
13. M. L. Free, A new corrosion inhibition model for surfactants that more closely accounts for actual adsorption than traditional models that assume physical coverage is proportional to inhibition, Corrosion Science, 10 May 2004.
14. M. Lagrenée, B. Mernari, M. Bouanis, M. Traisnel and F. Bentiss, Study of the mechanism and inhibiting efficiency of 3,5-bis(4-methylthiophenyl)-4H-1,2,4-triazole on mild steel corrosion in acidic media, Corrosion Science, Vol 44, Issue 3, March 2002.
15. ASTM G61, “Standard Test Method for Conducting Cyclic Potentiodynamic Polarization Measurements for Localized Corrosion Susceptibility of Iron-, Nickel-, or Cobalt-Based Alloys” (West Conshohocken, PA: ASTM).
16. ASTM G44, “Standard Practice for Exposure of Metals and Alloys by Alternate Immersion in 3.5% Sodium Chloride Solution” (West Conshohocken, PA: ASTM, 2003).
17. ASTM G48, “Standard Test Methods for Pitting and Crevice Corrosion Resistance of Stainless Steels and Related Alloys by Use of Ferric Chloride Solution” (West Conshohocken, PA: ASTM).
18. ASTM G106, “Standard Practice for Verification of Algorithm and Equipment for Electrochemical Impedance Measurements” (West Conshohocken, PA: ASTM).
19. ASTM G129, “Standard Practice for Slow Strain Testing to evaluate the susceptibility of metallic materials to Environmentally Assisted Cracking” (West Conshohocken, PA: ASTM 2003).